



**HAL**  
open science

## An anhydrous precursor approach to BaYF<sub>5</sub>-based upconverting nanocrystals

Bhagyesh Purohit, Erwann Jeanneau, Thibault Cornier, Gilles Ledoux, Shashank Mishra

► **To cite this version:**

Bhagyesh Purohit, Erwann Jeanneau, Thibault Cornier, Gilles Ledoux, Shashank Mishra. An anhydrous precursor approach to BaYF<sub>5</sub>-based upconverting nanocrystals. *Journal of the Indian Chemical Society*, 2022, 99 (2), pp.100322. 10.1016/j.jics.2021.100322 . hal-03681649

**HAL Id: hal-03681649**

**<https://hal.science/hal-03681649>**

Submitted on 8 Jan 2024

**HAL** is a multi-disciplinary open access archive for the deposit and dissemination of scientific research documents, whether they are published or not. The documents may come from teaching and research institutions in France or abroad, or from public or private research centers.

L'archive ouverte pluridisciplinaire **HAL**, est destinée au dépôt et à la diffusion de documents scientifiques de niveau recherche, publiés ou non, émanant des établissements d'enseignement et de recherche français ou étrangers, des laboratoires publics ou privés.



Distributed under a Creative Commons Attribution - NonCommercial 4.0 International License

## **An anhydrous precursor approach to BaYF<sub>5</sub>-based upconverting nanocrystals**

Bhagyesh Purohit,<sup>a</sup> Erwann Jeanneau,<sup>b</sup> Thibault Cornier,<sup>a</sup> Gilles Ledoux,<sup>c</sup> Shashank Mishra<sup>a\*</sup>

<sup>a</sup> Univ Lyon, Université Claude Bernard Lyon 1, CNRS, Institut de Recherches sur l'Environnement et la Catalyse de Lyon, 69626, Villeurbanne, France.

<sup>b</sup> Univ Lyon, Université Claude Bernard Lyon 1, Centre de Diffractométrie Henri Longchambon, 5 rue de La Doua, 69100 Villeurbanne, France.

<sup>c</sup> Univ Lyon, Université Claude Bernard Lyon 1, CNRS, Institut Lumière Matière, 69622, Villeurbanne, France.

E-mail: [shashank.mishra@ircelyon.univ-lyon1.fr](mailto:shashank.mishra@ircelyon.univ-lyon1.fr)

**Dedicated to (the late) Prof. Ram C. Mehrotra on the occasion of his birth centennial year**

### **Abstract**

With an objective to have easy access to high quality BaYF<sub>5</sub> matrix, we report here new anhydrous precursors of barium and yttrium which show a good compatibility in terms of co-thermal decomposition. These complexes not only fill the void of precursors for Ba-based upconverting (UC) nanomaterials but also provide a way to minimize the -OH concentration around these nanocrystals (NCs) to enhance their UC efficiency without requiring the usual core-shell structure. The precursors and the BaYF<sub>5</sub> NCs co-doped with Yb<sup>3+</sup>/Tm<sup>3+</sup> ions were thoroughly characterized. The NCs were studied for upconversion properties and preliminary results are presented here. On the basis of these results, a mechanism for the energy transfer in Yb-Tm system is proposed.

**Keywords:** Molecular precursor; Trifluoroacetate; Hot-injection; Anhydrous synthesis; BaYF<sub>5</sub>; Upconversion

## 1. Introduction

The lanthanide-based upconverting (UC) nanomaterials, which convert low energy IR photons to high energy UV-visible ones, are versatile materials that find many applications in different fields of science, including those in biosciences and photophysics [1-5]. However, a significant challenge in the field of UC nanomaterials is to enhance upconversion luminescence [6]. Quantum yields of lanthanide-doped UC NCs are extremely low- generally less than 1% of the conventional luminophores, and typically about an order of magnitude lower than those of corresponding UC bulk materials. It is a well-established fact now that –OH defects in the NCs are the primary cause of upconversion quenching [7]. The hydroxyl groups, which have vibrational frequency in the range 3000-3500 cm<sup>-1</sup>, generate more de-excitation pathways in the system, which results in the loss of UC emissions [8]. As the number of de-excitation pathways increases, it reduces the high energy UV-blue emissions, and increase low energy Red/NIR emission. Since more UV part is desired for the photocatalysis, it is essential to cut down on the quenching by OH groups. The usual strategy to minimize OH functionality on the NPs surface is to construct a shell of some inert materials, either SiO<sub>2</sub> or undoped matrix material [9-12]. However, for for certain applications such as photocatalysis [13], core-shell strategy is not desirable because it would increase the distance between the UC core and the photocatalyst and, therefore, would prevent an effective interaction between the two components. Moreover, presence of water may also replace F of the matrix due to similarity in ionic radii of O and F (i.e. formation of oxo-fluoride phase) [14].

Our strategy to address this problem has been to employ designed anhydrous molecular precursors, which allowed us to synthesize Yb and Tm co-doped GdF<sub>3</sub> or MM'F<sub>4</sub> nanocrystals

(M = Li, Na; M' = Y, Gd) with enhanced upconversion efficiency [15-19]. While the anhydrous conditions minimize –OH functionality on the surface of the upconverting NPs [19], the bottom-up synthesis using designed molecules generally facilitates a better control over the composition, structure and morphology of the nanomaterials [20-23]. Here we extend this approach to the BaYF<sub>5</sub>, which is one of the most suitable matrices for the co-doped Yb<sup>3+</sup> and Tm<sup>3+</sup> ions [24, 25]. As compared to Na-based host matrices NaLnF<sub>4</sub> (Ln = Y, Gd), there are very few studies on the synthesis of barium-based host matrices to date, and none of them is concerned with the molecular precursor approach [26-30]. While many anhydrous precursors of barium trifluoroacetates are known in the literature [31-35], they have mainly been used to get the metal oxide and their use as precursors to barium fluoride-based materials remains scarce [22]. Moreover, in the case of co-decomposition, compatibility between the two precursors in terms of similar thermal behaviour also becomes an important issue. In this article, we report anhydrous barium and lanthanide trifluoroacetate complexes with DMSO ligand, prepared via one-pot synthetic protocol using non-expensive commercially available reagents, which show a good thermal compatibility and codecompose in the same temperature range to afford BaYF<sub>5</sub> matrix. Doping this matrix with Yb<sup>3+</sup> and Tm<sup>3+</sup> ions afforded an efficient upconverting system, which was characterized by a range of characterization techniques and studied for the UC properties and energy transfer mechanism.

## **2. Results and discussion**

### *2.1. Synthesis and characterization of novel anhydrous molecular precursors*

As mentioned in the Introduction section, there is a clear void in the literature for the well-characterized molecular precursors for BaYF<sub>5</sub>-based up-converting nanomaterials. Metal trifluoroacetate complexes are the most easily available and the cheapest source for the metal fluoride/oxofluoride nanomaterials [22]. Anhydrous [Ba(TFA)<sub>2</sub>]<sub>∞</sub> can easily be prepared from

the reaction of BaH<sub>2</sub> and TFAH in methanol, but it is highly hygroscopic and not so soluble even in a coordinating solvent such as THF [33]. The hydrated [Ln(TFA)<sub>3</sub>(H<sub>2</sub>O)<sub>x</sub>] are commercially available, but can also be synthesized easily by reacting Ln<sub>2</sub>O<sub>3</sub> with trifluoroacetic acid under reflux. However, the presence of water molecules is detrimental to the luminescent properties of UC nanomaterials. As thermal dehydration of these hydrated complexes have proved difficult [36], the use of an ancillary co-ligand seems to be a preferred strategy to make them anhydrous. We and some other groups have previously demonstrated that the acyclic polyether glyme ligands or cyclic crown ethers not only replace the water molecules of hydrated metal trifluoroacetates to afford anhydrous precursors, but also stabilize metal complexes by wrapping/shielding the metal cations efficiently and saturating their coordination spheres, thus making them more air-stable and soluble in organic solvents [22]. In this work, we describe new anhydrous adducts of barium and yttrium trifluoroacetates with dimethyl sulfoxide (DMSO) ligand as potential precursors for BaYF<sub>5</sub>-based up-converting nanoparticles. As compared to the glyme or crown ether ligands, employing DMSO here has allowed us to use it both as a solvent and as an ancillary co-ligand in a straightforward one-pot synthesis of the anhydrous precursors. This has important implications in terms of producing these precursors on large scale for industrial applications.

A simple stirring of [Ba(TFA)<sub>2</sub>] and [Ln(TFA)<sub>3</sub>(H<sub>2</sub>O)<sub>x</sub>] in DMSO, followed by layering with toluene and dichloromethane, respectively, afforded crystals of new anhydrous precursors [Ba(TFA)<sub>2</sub>(DMSO)<sub>2</sub>] (**1**) and [Y(TFA)<sub>3</sub>(DMSO)<sub>2</sub>] (**2**) in good yield. Both compounds are readily soluble in DMSO, alcohols, THF as well as in long carbon chain organic solvents such as oleic acid or oleyl amine which are often used as high-boiling solvents during Metal organic Decomposition method to get NCs.

*2.1.1. Structural characterization of the precursors 1 and 2:* [Ba(TFA)<sub>2</sub>(DMSO)<sub>2</sub>]<sub>∞</sub> (**1**) crystallizes in monoclinic space group  $P\bar{1}$  and is a 1D straight chain polymer where barium

centers are bridged by four TFA and four DMSO ligands in an alternative manner (Figure 1). While all the DMSO ligands are bonded only in one fashion i.e.,  $\mu, \eta^1: \eta^1(\text{O}, \text{O})$ , the TFA ligands show two different bonding modes : two are bonded in  $\mu, \eta^1: \eta^1(\text{O}, \text{O}')$  and remaining two in  $\mu, \eta^2: \eta^1(\text{O}, \text{O}')$ . Each barium atom thus attains 9-coordination number. The dimethyl sulfoxide is a versatile ligand which may not only act in a terminal  $\eta^1(\text{O})$  or bridging  $\mu, \eta^1: \eta^1(\text{O})$  fashion but also in a amphidentate  $\mu, \eta^1: \eta^1(\text{O}, \text{S})$  manner to bind two different metal centers with different acidities [37]. The Ba1–O(TFA) bond lengths vary from 2.717(4) to 2.749(4) Å, and match well with the literature values [31-33]. The Ba–O (DMSO) bond distances [2.819(4)-2.843(3) Å] too are consistent with those reported for the related complexes with bridged DMSO [37]. As expected, bridging by four TFA ligands causes significant lengthening of the Ba···Ba distance [4.526 Å] as compared to 3.914 Å for Ba atoms bridged by four DMSO ligands. In contrast, the derivative  $[\text{Y}_2(\text{TFA})_6(\text{DMSO})_4]$  (**2**) is a discrete dinuclear molecule (Figure 2). The common  $\text{Y}_2(\mu, \eta^1, \eta^1\text{-TFA})_4(\eta^2\text{-TFA})_2$  core has two different coordination modes for the TFA ligand, namely chelating and bridging bidentate, the coordination sphere being completed by 2 DMSO ligands bonded in a terminal fashion to achieve nine-coordination for the each barium center. The Y–O bond lengths range from 2.269(8) to 2.511(9) Å, the order of variation being Y– $\eta^1$ -DMSO (av. 2.282 Å) < Y– $\mu$ -TFA (av. 2.337 Å) <  $\eta^2$ -TFA (av. 2.465 Å). The intramolecular Y···Y distance in the dimer is 4.493 Å. This dimeric structure can be related to those of  $[\text{Y}_2(\text{TFA})_6(\text{ROH})_x]$  [where R =  $\text{C}_2\text{H}_4\text{OPr}^i$  ( $x = 4$ ),  $\text{C}_2\text{H}_4\text{OC}_2\text{H}_4\text{OMe}$  ( $x = 2$ )] containing four  $\mu\text{-}\eta^1: \eta^1\text{-TFA}$  ligands [38].

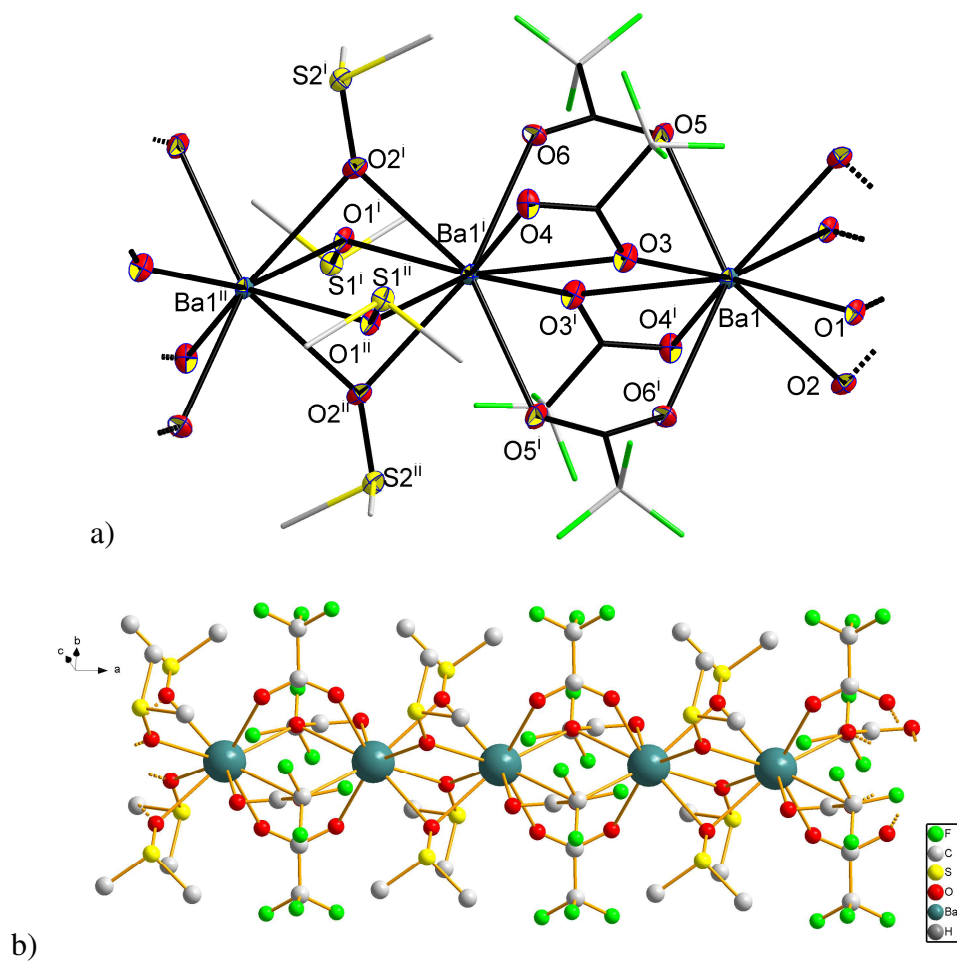


Figure 1. Perspective view of the X-ray structure of  $[\text{Ba}(\text{TFA})_2(\text{DMSO})_2]_\infty$  (**1**) with 50% probability ellipsoids. H atoms on DMSO ligands are omitted for clarity. (b) Extended structure of **1**. Symmetry elements: (i)  $-x, 1-y, 1-z$ ; (ii)  $-1+x, y, z$ . Selected bond lengths ( $\text{\AA}$ ) and angles ( $^\circ$ ): O1—Ba1 2.838(3), O2—Ba1 2.819(4), O3—Ba1 2.729(4), O5—Ba1 2.717(4), O2—Ba1—O1 61.60(10), O2—Ba1—O3 140.94(11), O1—Ba1—O3 93.92(11), O2—Ba1—O5 143.28(11), O1—Ba1—O5 128.10 (11), O3—Ba1—O5 75.65 (12).

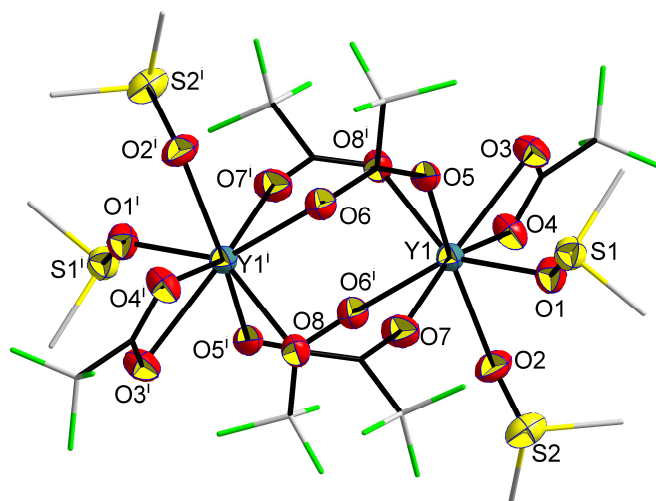


Figure 2. Perspective view of the X-ray structure of  $[Y(TFA)_3(DMSO)_2]_2$  (**2**) with 50% probability ellipsoids. H atoms on DMSO ligands are omitted for clarity. Symmetry element: (i)  $1-x, 1-y, 1-z$ . Selected bond lengths ( $\text{\AA}$ ) and angles ( $^\circ$ ): Y1—O1 2.269(8), Y1—O3 2.511(9), Y1—O8<sup>i</sup> 2.372(8), O1—Y1—O3 75.2(3), O1—Y1—O8<sup>i</sup> 143.2(3), O1—Y1—O4 98.3(3).

The FT-IR spectra of **1** and **2** show characteristic bands due to metal-bonded TFA and DMSO ligands [39]. The stretching frequency of the C=O bond differs for solely bridging, chelating or both bridging and chelating TFA ligand. The appearance of a single but relatively broad peak in the region  $1520\text{--}1834\text{ cm}^{-1}$  for **1** and **2** is probably due to overlapping of the  $\nu(\text{CO}_2)$  absorption of the two different bonding modes of the TFA ligand present in these precursors. While the frequencies around  $1110\text{--}1210\text{ cm}^{-1}$  confirm the presence of C-F and C-O bonds, three other characteristic absorptions for TFA ligand were found in the  $842\text{--}716\text{ cm}^{-1}$  region. An intense  $\nu(\text{S-O})$  also appears at  $1008\text{--}1022\text{ cm}^{-1}$ , showing a significant shift from the same absorption at  $1056\text{ cm}^{-1}$  in free DMSO molecule. As expected, the  $^1\text{H}$  NMR spectra of **1** and **2** in  $\text{CDCl}_3$  are simple and show only a singlet at  $\delta$  1.61 and 1.62 ppm, respectively, for the methyl groups of the DMSO ligand.

**2.1.2. Thermogravimetric analysis.** The thermal behaviour of the new anhydrous barium and yttrium trifluoroacetate precursors was investigated under an argon atmosphere in the  $20\text{--}600$

°C temperature range by thermogravimetric analysis (TGA). The barium derivative **1** shows a 2-step decomposition, with two important endothermic peaks appearing at 228 and 331 °C in the DTG curve (Figure 3a). The remaining residue weight (~32% at 350 °C) accounts for a little less than the expected yield of BaF<sub>2</sub> materials (33.7%), probably due to some volatility of the product. On the other hand, the TG-DTG curves of the yttrium precursor **2** shows predominantly one-step decomposition in the range 250-310 °C, as indicated by a prominent endothermic DTG peak at 308 °C (Figure 3b). The remaining weight of the residue is consistent with the formation of YF<sub>3</sub> as the end product (~26% observed at 350 °C versus 25% theoretical). Thermal decomposition of some related barium and yttrium trifluoroacetates in an inert atmosphere to BaF<sub>2</sub> and YF<sub>3</sub>, respectively, has been shown previously [40]. Despite of different decomposition patterns, the two complexes **1** and **2** show a good compatibility in their decomposition temperature range, suggesting that these precursors can be co-decomposed to get the BaYF<sub>5</sub> matrix.

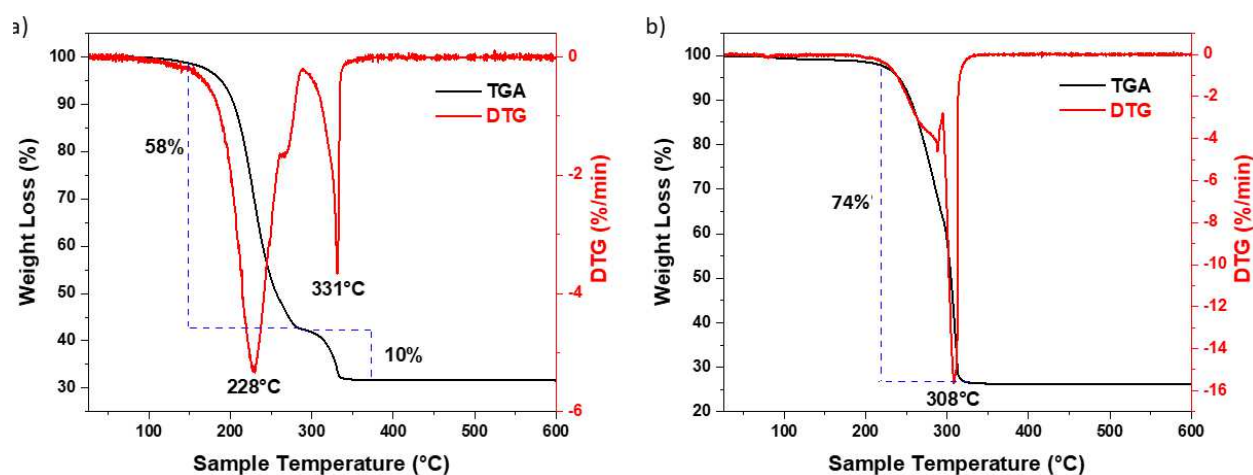


Figure 3. TG-DTG curves of (a) [Ba(TFA)<sub>2</sub>(DMSO)<sub>2</sub>] (**1**), and (b) [Y(TFA)<sub>3</sub>(DMSO)<sub>2</sub>]<sub>2</sub> (**2**).

## 2.2. Synthesis of undoped and Yb<sup>3+</sup>, Tm<sup>3+</sup> co-doped BaYF<sub>5</sub> nanocrystals from the thermal decomposition of anhydrous precursors

2.2.1. *Synthesis of undoped BaYF<sub>5</sub> matrix.* The upconversion process is significantly dependent on the choice of host matrix, as it can exert a crystal field around the dopant ions and modify the excitation energy of dopant through lattice vibrations [41]. Hence, it is necessary to choose a perfect host matrix that promises very low phonon energy and non-radiative relaxation emission. The barium-based matrix BaLnF<sub>5</sub> (Ln = Y, Gd) are promising host matrices for NIR to UV upconversion because of their ideal phonon energies which are suitable for aiding energy transfer and multiphonon relaxation processes, yet not so small that can cause multiphonon-assisted relaxations [24]. For instance, the BaYF<sub>5</sub> matrix was found to be nearly 8 times more efficient in comparison to LnF<sub>3</sub> for studying the upconversion emission from co-doped Yb-Er ions [42]. Following TGA studies of **1** and **2** which showed a good compatibility in thermal behaviour, we co-decomposed an equivalent mixture of these two anhydrous precursors in a 1:1 solution of 1-octadecene (ODE) and oleic acid (OA) at 310 °C. As expected, this decomposition resulted in the formation of phase pure and well crystalline tetragonal BaYF<sub>5</sub> nanoparticles as indicated by its powder XRD pattern that corresponds to PDF # 00-046-0039.

2.2.2. *Synthesis of Yb<sup>3+</sup>, Tm<sup>3+</sup> doped BaYF<sub>5</sub> NCs.* A fine balance of concentration of both dopants (sensitizer Yb<sup>3+</sup> and activator Tm<sup>3+</sup>) is needed to maximize the upconversion emission because if the concentration of the dopants (Yb<sup>3+</sup>/Tm<sup>3+</sup>) is less, then the full UC potential cannot be observed. On the other hand, even a slight excess of these dopant ions can reduce the UC emission to a great extent due to the phenomenon called concentration quenching [43]. Based on our previous studies [19] as well as reports available in the literature [43], we chose 20 mol% and 0.5 mol% as the doping concentration of the sensitizer (Yb<sup>3+</sup>) and the activator (Tm<sup>3+</sup>), respectively. To co-dope the host matrix BaYF<sub>5</sub> with up-converting ytterbium and thulium cations, analogous anhydrous lanthanide complexes [Ln(TFA)<sub>3</sub>(DMSO)<sub>2</sub>] (Ln = Tm and Yb) were also prepared by reacting Ln(TFA)<sub>3</sub>(H<sub>2</sub>O)<sub>x</sub> with

DMSO, and subsequently precipitating the desired products by adding dichloromethane. The FT-IR spectra and elemental analyses of the obtained white powders confirmed their composition as  $[\text{Ln}(\text{TFA})_3(\text{DMSO})_2]$  ( $\text{Ln} = \text{Tm}$  and  $\text{Yb}$ ). Subsequently, the synthesis of  $\text{Yb}^{3+}$ ,  $\text{Tm}^{3+}$  doped  $\text{BaYF}_5$  NCs was achieved by simultaneous thermal decomposition of appropriate amounts of  $[\text{Ba}(\text{TFA})_2(\text{DMSO})_2]$  and  $[\text{Ln}(\text{TFA})_3(\text{DMSO})_2]$  ( $\text{Ln} = \text{Y}$ ,  $\text{Yb}$ ,  $\text{Tm}$ ) and in a mixture of ODE and OA. Figure 4a depicts the powder X-ray diffraction patterns of the as-obtained powder, which correspond to the phase-pure and well-crystalline  $\text{BaYF}_5$  (PDF # 00-046-0039). Their TEM and HR-TEM images show them to be agglomerated but well-crystalline particles of sub-20 nm size (Figure 4c-d). The associated FFT analysis, shown as inset of the Figure 4d, is consistent with the (330) and (131) crystal planes of the tetragonal  $\text{BaYF}_5$  (PDF # 00-046-0039). The presence of oleic acid as capping ligand around these NCs is confirmed by the FTIR and TG-DTG studies (Figures 4c and 4d). The FT-IR spectrum exhibits strong absorptions due to i)  $\nu\text{O-H}$  stretching vibrations in the region  $3500\text{-}3800\text{ cm}^{-1}$ , ii) the symmetric and asymmetric stretching of the methylene ( $\text{CH}_2$ ) groups at  $2868$  and  $2926\text{ cm}^{-1}$ , respectively, and iii) the asymmetric and symmetric stretching vibrations of  $\text{C=O}$  at  $1548$  and  $1457\text{ cm}^{-1}$ , respectively (Figure 4c). The TG-DTG curves show  $\sim 23\%$  weight loss in the temperature range  $350\text{-}500\text{ }^\circ\text{C}$  with a strong endothermic peak appearing at  $440\text{ }^\circ\text{C}$  (Figure 4d).

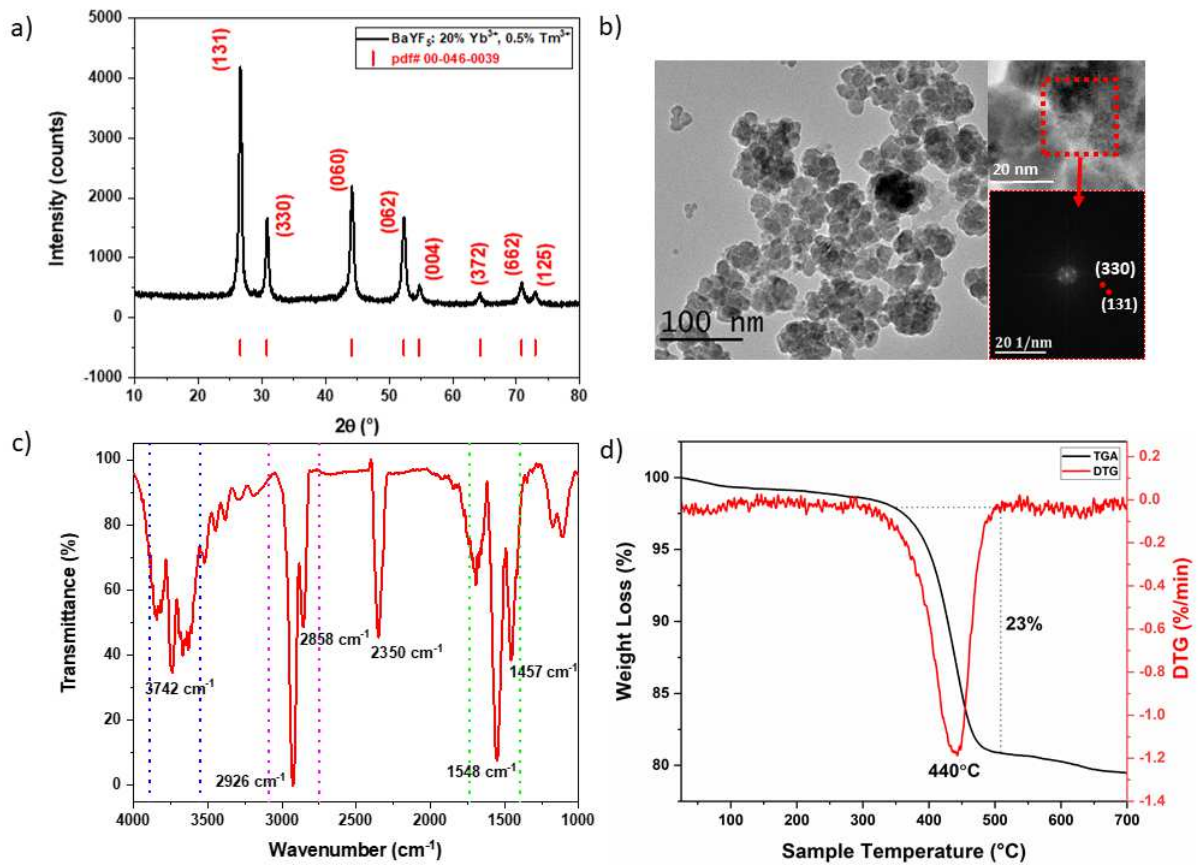


Figure 4. Characterization of  $\text{BaYF}_5: \text{Yb}^{3+}, \text{Tm}^{3+}$  NCs : (a) XRD, (b) TEM and HR-TEM images with associated FFT, (c) FT-IR spectrum, and (d) TGA-DTG curves.

### 2.3. Upconversion studies of $\text{BaYF}_5: \text{Yb}^{3+}, \text{Tm}^{3+}$ nanocrystals

The power dependent upconversion spectra of the  $\text{BaYF}_5: \text{Yb}^{3+}, \text{Tm}^{3+}$  NCs under an excitation of 973 nm show upconversion from NIR to UV from different energy levels of  $\text{Tm}^{3+}$  ions (Figure 5a). While the UV peak around 360 nm corresponds to the  $^1\text{D}_2$  to ground level emission, those at 470, 640 and 800 nm correspond to the emission from  $^1\text{G}_4$ ,  $^3\text{F}_{2,3}$  and  $^3\text{H}_4$ , respectively, down to the ground state  $^3\text{H}_6$ . The series of peak around 670-720 nm correspond to the emission from  $^1\text{G}_4$  down to the two first excited states ( $^3\text{F}_4$ ,  $^3\text{H}_5$ ). These transitions are consistent with those reported in the literature [24,29]. Figure 5b presents the intensity evolution of three emissions of  $\text{Tm}^{3+}$  by upconversion, where one can observe that

below  $10\text{W/cm}^2$  the evolution of the intensity follows a nonlinear evolution with a power 2 and 3, respectively, for the  ${}^3\text{H}_4 \rightarrow {}^3\text{H}_6$  and  ${}^1\text{G}_4 \rightarrow {}^3\text{H}_6$  transitions.

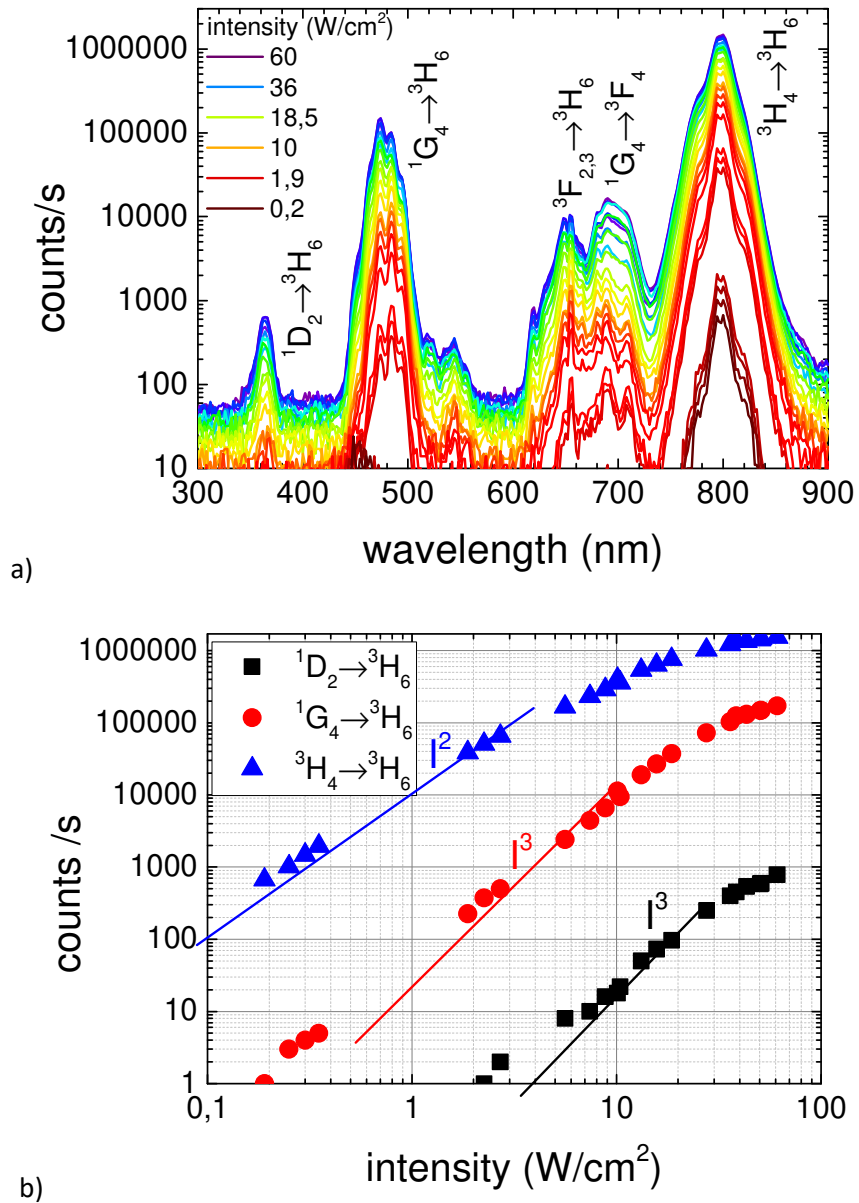


Figure 5. Upconversion spectra of  $\text{BaYF}_5:\text{Yb}^{3+}, \text{Tm}^{3+}$ : a) UC luminescence under an excitation of 973 nm at different intensities, and b) intensity evolution of three main UC emissions.

The energy transfer mechanism in Yb-Tm system is not very clear yet, so, these class of NCs could be very beneficial to understand the exact energy transfer process between  $\text{Yb}^{3+}$  and  $\text{Tm}^{3+}$  ions. Usually,  $\text{Tm}^{3+}$  ions in  $\text{BaYF}_5$  matrix does not have any energy levels that

match well with the excitation source of 973 nm laser (Figure 6). This suggests that the first transition should occur in the  $\text{Yb}^{3+}$  ions with an incoming photon of 973 nm CW laser exciting the electron from the  $^2\text{F}_{7/2}$  to  $^2\text{F}_{5/2}$  energy levels. The excited Yb would decay non-radiatively and transfer the energy to the nearby  $\text{Tm}^{3+}$  ion to populate its  $^3\text{H}_5$  energy level. This is followed by subsequent non-radiative phonon decay (dashed line in Figure 6) which populates the  $^3\text{F}_4$  energy levels of  $\text{Tm}^{3+}$  (Step a, Figure 6). A second incoming (973 nm) photon or the energy transfer from the  $\text{Yb}^{3+}$  ion can populate the  $^3\text{F}_{2,3}$  levels, which in turn can populate the  $^3\text{H}_4$  energy level by non-radiative relaxation (Step b, Figure 6). The ground relaxation from this energy level ( $^3\text{H}_4 \rightarrow ^3\text{H}_6$ ) is responsible for the peak around 800 nm in Figure 5. Furthermore, a third incoming photon or the energy transfer from the  $\text{Yb}^{3+}$  ion can populate the  $^1\text{G}_4$  and higher energy levels (Step c, Figure 6). The transition of electrons from this level to the lower  $^3\text{F}_4$  and  $^3\text{H}_5$  levels result in the weak red emissions at ~670 nm and ~710 nm. The population of the  $^1\text{D}_2$  level follows probably a different route. As can be seen in the Figure 5b, it also follows a power of 3 dependencies. This could be explained if the level is populated through the combined transfer of two Yb excited ion from the  $^3\text{F}_4$  to the  $^1\text{D}_2$  level (Step d, Figure 6). Even if this process has a lower probability, it is still possible due to two factors i.e., at the high doping level of Yb, the probability of having two nearby excited Yb ions at intensities above  $1\text{W}/\text{cm}^2$  is rather high, and the transition  $^3\text{F}_4 \rightarrow ^1\text{D}_2$  is extremely strong [18].

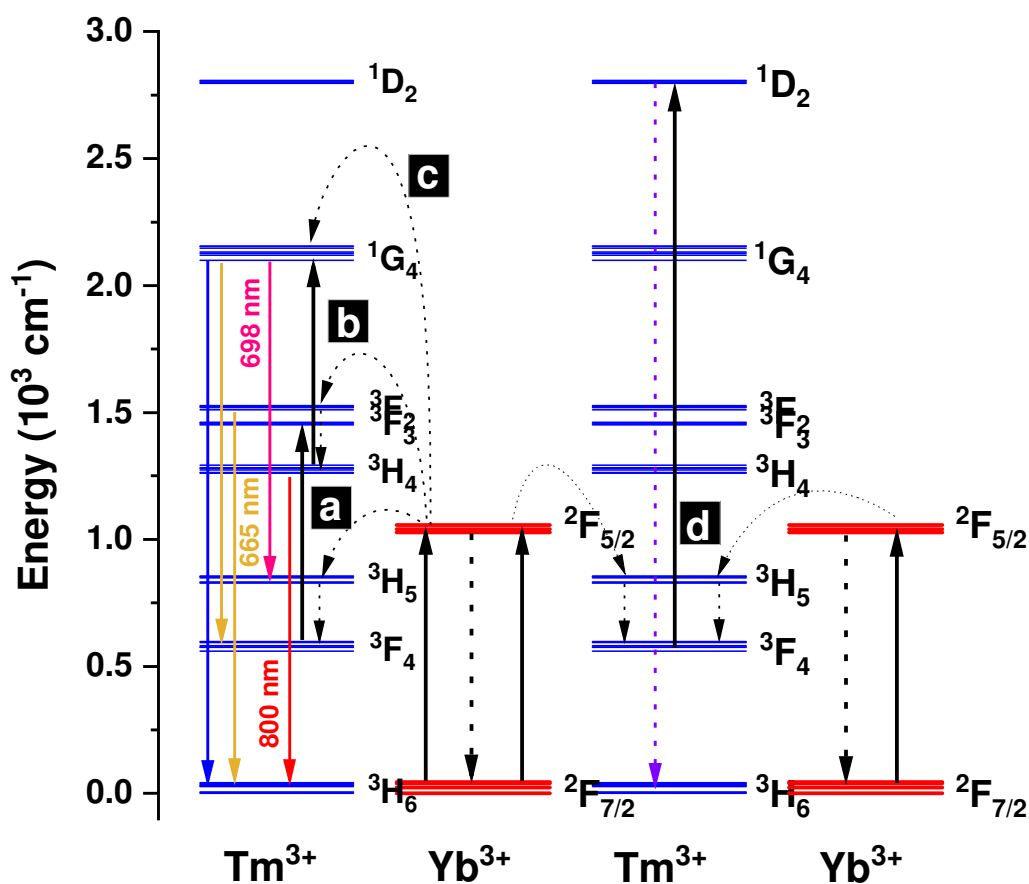


Figure 6. Upconversion mechanism and energy level scheme for Yb<sup>3+</sup> and Tm<sup>3+</sup> co-doped BaYF<sub>5</sub> NCs.

### 3. Materials and methods

**3.1. General Procedures.** The syntheses and decomposition of the precursors were carried out under argon using Schlenk tube and vacuum line techniques. Solvents were purified on an MB SPS-800 instrument. The starting reactants [Ba(TFA)<sub>2</sub>] and [Ln(TFA)<sub>3</sub>(H<sub>2</sub>O)<sub>3</sub>] (Ln = Y, Tm, Yb) were prepared following the procedures described in the literature [15, 33]. Trifluoroacetic acid (TFAH) and DMSO (both Aldrich) were stored over molecular sieves, whereas 1-octadecene and oleic acid (both Aldrich) were used as received. FT-IR spectra of the new anhydrous precursors (as Nujol mulls) and nanocrystals (as KBr pallets) were recorded on a Bruker Vector 22 spectrometer. <sup>1</sup>H NMR spectra were recorded in CDCl<sub>3</sub> on a Bruker AC-300 spectrometer. The TG-DTA data of **1** and **2** were collected in argon

atmosphere (flow rate 50 cm<sup>3</sup>/min, thermal ramp 5 °C/min, temperature range 20-600 °C) using a SETSYS Evolution-12 thermal analyzer. Powder X-ray diffraction data were obtained with a Siemens D 5000 diffractometer using CuK $\alpha$  radiation. Transmission electron microscopy (TEM) was performed on a JEOL JEM-2100 LaB $_6$  microscope operated at 200 kV. Upconverting studies were made on a homemade spectrofluorimeter. The samples were irradiated with a continuous wave (CW) laser at 973 nm which was focused to a square spot of 1x1 mm<sup>2</sup> on the sample with a quasi-top-hat energy distribution. All the measurements were performed under similar conditions at variable excitation power density. The intensities of excitation were varied using different optical density filters. The emitted signal was then collected using Jobin-Yvon (TRIAX 320) monochromator equipped with automatic order removing filters and coupled to a cooled photomultiplier (Hamamatsu R943-02). The signal from the photomultiplier was sent to an SR400 counting module from Stanford Research Systems.

### 3.2. Synthesis of new complexes:

**[Ba(TFA)<sub>2</sub>(DMSO)<sub>2</sub>] (1)**. [Ba(TFA)<sub>2</sub>] (0.58 g, 1.59 mmol) was stirred in DMSO (4 mL) for 1h, which led to a change in color of the solution from colorless to light yellow. The solution was then concentrated to 2 mL and layered with 6 ml of toluene, which resulted in colorless crystals of **1**. The crystallized product was then isolated by separating it from mother solution and was subsequently washed with cold *n*-pentane. Yield, 0.65 g (78%). Anal. Calcd. for C<sub>8</sub>H<sub>12</sub>BaF<sub>6</sub>O<sub>6</sub>S<sub>2</sub> (519.65): C, 18.47; H, 2.30; Found: C, 18.73; H, 2.37%. FT-IR (Nujol, cm<sup>-1</sup>): 3590-3100br, 2924s, 2722w, 2613w, 2505w, 2382w, 2348w, 2316w, 2278w, 2239w, 1976m, 1834-1520br, 1440s, 1376s, 1320s, 1210-1110s, 1022s, 959s, 939s, 900s, 842s, 800s, 716s, 676s, 597m, 518m, 411m. <sup>1</sup>H NMR (300 MHz, CDCl<sub>3</sub>, ppm):  $\delta$  = 1.61 (s, 12 H, CH<sub>3</sub>).

By adopting the similar procedure, stirring of  $[Y(TFA)_3(H_2O)_3]$  (0.50 g, 1.05 mmol) in 2 ml of DMSO for 1h, followed by layering the solution with dichloromethane gave  $[Y(TFA)_3(DMSO)_2]$  (**2**) as colorless complex in 85% yield (0.52 g). Anal. Calcd. for  $C_{20}H_{24}F_{18}O_{16}S_4Y_2$  (1168.45): C, 20.54; H, 2.05; Found: C, 20.17; H, 1.97%. FT-IR (Nujol,  $cm^{-1}$ ): 3600-3050m, 2970-2912m, 2620-2580w, 2384w, 2349w, 1975w, 1834-1520s, 1438s, 1378m, 1318s, 1199s, 1130s, 1008s, 906w, 803m, 799s, 720s, 672w, 601m, 520m, 421m.  $^1H$  NMR (300 MHz,  $CDCl_3$ ):  $\delta = 1.62$  (s, 24 H,  $CH_3$ ).

**3.3. X-Ray Crystallography.** Suitable crystals of **1** and **2** were obtained as described in the experimental section. Crystals structure were determined an Xcalibur Gemini kappa-geometry diffractometer equipped with an Atlas CCD and a Molybdenum X-ray source ( $\lambda = 0.71073 \text{ \AA}$ ). Intensities were collected by means of the CrysAlisPro software [44]. Reflection indexing, unit-cell parameters refinement, Lorentz-polarization correction, peak integration and background determination were carried out with the CrysAlisPro software [44]. An analytical absorption correction was applied using the modeled faces of the crystal [45]. The resulting set of  $hkl$  was used for structure solution and refinement. The structures were solved with the ShelXT [46] structure solution program using the intrinsic phasing solution method and by using Olex2 [47] as the graphical interface. The model was refined with version 2018/3 of ShelXL [46] using least-squares minimization. Some selected crystallographic and refinement data of the molecular complexes **1** and **2** are listed in Table 1.

Table 1. Selected crystallographic and refinement data of **1** and **2**.

	<b>1</b>	<b>2</b>
Empirical formula	$C_8H_{12}BaF_6O_6S_2$	$C_{20}H_{24}F_{18}O_{16}S_4Y_2$
Formula weight	519.65	1168.45
Crystal system	Triclinic	Orthorhombic
Space group	$P\bar{1}$	$Pbca$
a (Å)	8.4266 (9)	14.479(3)
b (Å)	9.9849 (9)	16.1312(19)
c (Å)	10.5275 (9)	17.502(3)
$\alpha$ (°)	108.622 (8)	90

$\beta$ (°)	102.277 (9)	90
$\gamma$ (°)	92.599 (8)	90
V (Å <sup>3</sup> )	814.04 (14)	4087.7(10)
Z	2	4
$\mu$ (mm <sup>-1</sup> )	2.78	3.172
Temperature (K)	100	150
Measured reflns	14480	29466
Indep/obsd [ $I > 2\sigma(I)$ ] reflns	4056/3758	5205/2937
R <sub>int</sub>	0.068	0.1542
Restraints/parameters	0/208	0/275
GOF	1.00	1.047
wR <sub>2</sub>	0.046	0.3038
R <sub>1</sub>	0.121	0.1220
Residual electron density (e/Å <sup>-3</sup> )	-1.92 to 2.07	-1.183 to 5.159
CCDC no.	2107287	2109390

### 3.4. Anhydrous synthesis of undoped BaYF<sub>5</sub> and doped BaYF<sub>5</sub>:Yb<sup>3+</sup>, Tm<sup>3+</sup> nanocrystals.

To obtain undoped BaYF<sub>5</sub> nanocrystals, 0.6 mmol each of [Ba(TFA)<sub>2</sub>(DMSO)<sub>2</sub>] (**1**) and [Y(TFA)<sub>3</sub>(DMSO)<sub>2</sub>] (**2**) were taken in a mixture of 2 ml each of 1-octadecene (ODE) and oleic acid (OA) and heated to 120 °C to obtain a clear solution (batch A). In parallel, a mixture of 2 ml each of ODE + OA was purged with argon and heated to 300 °C (batch B). When the temperature became constant at 310 °C for batch B, the pre-heated batch A was injected in batch B all at once. The reaction mixture was then stirred at 310 °C for 1h. It was then gradually cooled down to room temperature under a constant flow of argon. To collect the nanocrystals, ethanol was added as a precipitating agent, followed by centrifugation at 4500 rpm for 5 min. The resulting powder was washed two times with ethanol and one time with *n*-pentane to remove any organic impurities and then air-dried at room temperature for 24h.

To prepare BaYF<sub>5</sub>:Yb<sup>3+</sup>, Tm<sup>3+</sup> NCs, appropriate amounts of [Ba(TFA)<sub>2</sub>(DMSO)<sub>2</sub>], [Y(TFA)<sub>3</sub>(DMSO)<sub>2</sub>], [Yb(TFA)<sub>3</sub>(DMSO)<sub>2</sub>] and [Tm(TFA)<sub>3</sub>(DMSO)<sub>2</sub>] were taken in a mixture of ODE + OA and simultaneously decomposed as described above.

#### **4. Conclusions**

As compared to the traditional solution or solid-phase synthetic methods of nanoparticles, the precursor-controlled synthesis enjoys many advantages such as requiring a milder condition [48] or exerting a better control over the stoichiometry, phase, size and shape of the particles [20-23]. In this article, we described synthesis and characterization of two novel anhydrous molecular precursors which co-decompose in a similar temperature window to afford high quality upconverting BaYF<sub>5</sub>:Yb<sup>3+</sup>, Tm<sup>3+</sup> nanocrystals. A mechanism for the energy transfer in Yb-Tm system is proposed on the basis of the upconversion properties of these NCs. Further work on upconversion quantum yield measurement on these UC NCs is currently underway.

#### **Acknowledgements**

This work was supported by the Agence Nationale de la Recherche through the grant number ANR-17-CE09-0002. The authors thank Y. Aizac of IRCELYON for powder XRD data.

#### **Funding**

This work was supported by the Agence Nationale de la Recherche through the grant number ANR-17-CE09-0002.

#### **Declaration of Competing Interest**

There are no interests to declare.

#### **References**

[1] Zheng, K.; Loh, K. Y.; Wang, Y.; Chen, Q.; Fan, J.; Jung, T.; Nam, S. H.; Suh, Y. D.; Liu, X. Recent advances in upconversion nanocrystals: Expanding the kaleidoscopic toolbox for emerging applications, *Nano Today* **2019**, *29*, 100797.

- [2] Wen, S.; Zhou, J.; Zheng, K.; Bednarkiewicz, A.; Liu, X.; Jin, D. Advances in highly doped upconversion nanoparticles. *Nat. Commun.* **2018**, *9*, 2415.
- [3] Li, X.; Zhang, F.; Zhao, D. Lab on upconversion nanoparticles: Optical properties and applications engineering via designed nanostructure. *Chem. Soc. Rev.* **2015**, *44*, 1346–1378.
- [4] Yang, D.; Ma, P.; Hou, Z.; Cheng, Z.; Li, C.; Lin, J. Current advances in lanthanide ion ( $\text{Ln}^{3+}$ )-based upconversion nanomaterials for drug delivery. *Chem. Soc. Rev.* **2015**, *44*, 1416–1448.
- [5] Zhou, J.; Liu, Q.; Feng, W.; Sun, Y.; Li, F. Upconversion luminescent materials: Advances and applications. *Chem. Rev.* **2015**, *115*, 395–465.
- [6] Tessitore, G.; Mandl, G. A.; Brik, M. G.; Park, W.; Capobianco, J. A. Recent insights into upconverting nanoparticles: Spectroscopy, modeling, and routes to improved luminescence. *Nanoscale* **2019**, *11*, 12015–12029.
- [7] Wang, Z.; Meijerink, A. Concentration quenching in upconversion nanocrystals. *J. Phys. Chem. C* **2018**, *122*, 26298–26306.
- [8] R. Arppe, I. Hyppanen, N. Perala, R. Peltomaa, M. Kaiser, C. Wurth, S. Christ, U. Resch-Genger, M. Schaferling, T. Soukka, Quenching of the upconversion luminescence of  $\text{NaYF}_4:\text{Yb}^{3+},\text{Er}^{3+}$  and  $\text{NaYF}_4:\text{Yb}^{3+},\text{Tm}^{3+}$  nanophosphors by water: the role of the sensitizer  $\text{Yb}^{3+}$  in non-radiative relaxation, *Nanoscale* **2015**, *7*, 11746–11757.
- [9] Chen, X.; Peng, D.; Ju, Q.; Wang, F. Photon Upconversion in core–shell nanoparticles. *Chem. Soc. Rev.* **2015**, *44*, 1318–1330.
- [10] Vetrone, F.; Naccache, R.; Mahalingam, V.; Morgan, C. G.; Capobianco, J. A. The active-core/active-shell approach: A strategy to enhance the upconversion luminescence in lanthanide-doped nanoparticles. *Adv. Funct. Mater.* **2009**, *19*, 2924–2929.

- [11] Li, X.; Shen, D.; Yang, J.; Yao, C.; Che, R.; Zhang, F.; Zhao, D. Successive layer-by-layer strategy for multi-shell epitaxial growth: Shell thickness and doping position dependence in upconverting optical properties. *Chem. Mater.* **2013**, *25*, 106–112.
- [12] Cao, C.; Liu, Q.; Shi, M.; Feng, W.; Li, F. Lanthanide-doped nanoparticles with upconversion and downshifting near-infrared luminescence for bioimaging. *Inorg. Chem.* **2019**, *58*, 9351–9357.
- [13] Zhang, Q.; Yang, F.; Xu, Z.; Chaker, M.; Ma, D. Are lanthanide-doped upconversion materials good candidates for photocatalysis? *Nanoscale Horiz.* **2019**, *4*, 579–591.
- [14] Du, Y.-P.; Zhang, Y.-W.; Sun, L.-D.; Yan, C.-H. Luminescent monodisperse nanocrystals of lanthanide oxyfluorides synthesized from trifluoroacetate precursors in high-boiling solvents, *J. Phys. Chem. C* **2008**, *112*, 405-415.
- [15] a) Mishra, S.; Ledoux, G.; Jeanneau, E.; Daniele, S.; Joubert, M.-F. Novel heterometal-organic complexes as first single source precursors for up-converting NaYF<sub>4</sub>:Yb<sup>3+</sup>, Er<sup>3+</sup>/Tm<sup>3+</sup> nanomaterials, *Dalton Trans.*, **2012**, *41*, 1490–1502; b) Mishra, S.; Daniele, S.; Ledoux, G.; Jeanneau, E.; Joubert, M.-F. Heterometallic Na-Y(Ln) trifluoroacetate diglyme complexes as novel single source precursors for upconverting NaYF<sub>4</sub> nanocrystals co-doped with Yb and Er/Tm ions, *Chem. Commun.*, **2010**, *46*, 3756–3758.
- [16] Chen, Y.; Mishra, S.; Ledoux, G.; Jeanneau, E.; Daniel, M.; Zhang, J.; Daniele, S. Direct synthesis of hexagonal NaGdF<sub>4</sub> nanocrystals from a single-source precursor: Upconverting NaGdF<sub>4</sub>:Yb<sup>3+</sup>,Tm<sup>3+</sup> and its composites with TiO<sub>2</sub> for near-IR-driven photocatalysis. *Chem. Asian J.* **2014**, *9*, 2415–2421.
- [17] Ayadi, H.; Fang, W.; Mishra, S.; Jeanneau, E.; Ledoux, G.; Zhang, J.; Daniele, S. Influence of Na<sup>+</sup> ion doping on the phase change and upconversion emissions of the GdF<sub>3</sub>:Yb<sup>3+</sup>, Tm<sup>3+</sup> nanocrystals obtained from the designed molecular precursors, *RSC Adv.*, **2015**, *5*, 100535-100545.

- [18] Purohit, B.; Guyot, Y.; Amans, D.; Joubert, M.-F.; Mahler, B.; Mishra, S.; Daniele, S.; Dujardin, C.; Ledoux, G. Multicolor solar absorption as a synergetic UV upconversion enhancement mechanism in  $\text{LiYF}_4:\text{Yb}^{3+},\text{Tm}^{3+}$  nanocrystals, *ACS Photonics* **2019**, *6*, 3126-3131.
- [19] Purohit, B.; Amans, D.; Guyot, Y.; Mahler, B.; Joubert, M.-F.; Dujardin, C.; Daniele, S.; Ledoux, G.; Mishra, S. Quest to enhance up-conversion efficiency: A comparison of anhydrous versus hydrous synthesis of  $\text{NaGdF}_4:\text{Yb}^{3+},\text{Tm}^{3+}$  nanoparticles, *Mater. Today. Chem.* **2020**, *17*, 100326.
- [20] Brune, V.; Grosch, M.; Weißing, R.; Hartl, F.; Frank, M.; Mishra, S.; Mathur, S. Influence of the choice of precursors in the synthesis of two dimensional transition metal dichalcogenides, *Dalton Trans.* **2021**, *50*, 12365-12385.
- [21] Mishra, S.; Daniele, S. Molecular engineering of metal alkoxides for solution phase synthesis of high-tech metal oxide nanomaterials, *Chem. Eur. J.* **2020**, *26*, 9292–9303.
- [22] Mishra, S.; Daniele, S. Metal-organic derivatives with fluorinated ligands as precursors for inorganic nanomaterials, *Chem. Rev.* **2015**, *115*, 8379-8448.
- [23] Mishra, S.; Daniele, S.; Hubert-Pfalzgraf, L. G. Metal 2-ethylhexanoates and related compounds as useful precursors in materials science, *Chem. Soc. Rev.* **2007**, *36*, 1770–1787.
- [24] Vetrone, F.; Mahalingam, V.; Capobianco, J. A. Near-infrared-to-blue upconversion in colloidal  $\text{BaYF}_5:\text{Tm}^{3+},\text{Yb}^{3+}$  nanocrystals. *Chem. Mater.* **2009**, *21*, 1847–1851.
- [25] Maurizio, S. L.; Tessitore, G.; Krämer, K. W.; Capobianco, J. A.  $\text{BaYF}_5:\text{Yb}^{3+},\text{Tm}^{3+}$  Upconverting nanoparticles with improved population of the visible and near-infrared emitting states: Implications for bioimaging, *ACS Appl. Nano Mater.* **2021**, *4*, 5301–5308.
- [26] Luo, R.; Chen, L.; Li, Q.; Zhou, J.; Mei, L.; Ning, Z.; Zhao, Y.; Liu, M.; Lai, X.; Bi, J.; Yin, W.; Gao, D.  $\text{Bi}^{3+}$ -Doped  $\text{BaYF}_5:\text{Yb},\text{Er}$  upconversion nanoparticles with enhanced

luminescence and application case for X-ray computed tomography imaging. *Inorg. Chem.* **2020**, *59*, 17906–17915.

[27] Shao, W.; Sun, Z.; Hua, R.; Zhang, W.; Zhao, J.; Na, L. Bioconjugation of poly (acrylic acid)-capped BaYF<sub>5</sub>:Yb<sup>3+</sup>/Er<sup>3+</sup> up-conversion nanoparticles to bovine serum albumin: Synthesis

[28] Pan, S.; Deng, R.; Feng, J.; Song, S.; Wang, S.; Zhu, M.; Zhang, H. Microwave-assisted synthesis and down- and up-conversion luminescent properties of BaYF<sub>5</sub>:Ln (Ln = Yb/Er, Ce/Tb) nanocrystals. *CrystEngComm* **2013**, *15*, 7640.

[29] Niu, N.; Yang, P.; Liu, Y.; Li, C.; Wang, D.; Gai, S.; He, F. Controllable synthesis and up-conversion properties of tetragonal BaYF<sub>5</sub>:Yb/Ln (Ln = Er, Tm, and Ho) nanocrystals. *J. Colloid Interface Sci.* **2011**, *362*, 389–396.

[30] Zhang, C.; Ma, P.; Li, C.; Li, G.; Huang, S.; Yang, D.; Shang, M.; Kang, X.; Lin, J.; Controllable and white upconversion luminescence in BaYF<sub>5</sub>:Ln<sup>3+</sup> (Ln = Yb, Er, Tm) nanocrystals, *J. Mater. Chem.* **2011**, *21*, 717–723.

[31] Mishra, S.; Zhang, J.; Hubert-Pfalzgraf, L. G.; Luneau, D.; Jeanneau, E. The Interplay between yttrium, barium or copper trifluoroacetates and *N*-methyldiethanolamine: Synthesis of a heterometallic Y<sub>3</sub>Cu trifluoroacetate complex and a homometallic Ba-TFA 1D polymer, *Eur. J. Inorg. Chem.* **2007**, 602–608.

[32] Boyle, T. J.; Pratt, H. D.; Alam, T. M.; Rodriguez, M. A.; Clem, P. G. Synthesis and characterization of solvated trifluoroacetate alkaline earth derivatives, *Polyhedron* **2007**, *26*, 5095–5103.

[33] Zhang, J.; Hubert-Pfalzgraf, L. G.; Luneau, D. Synthesis, characterization and molecular structures of Cu(II) and Ba(II) fluorinated carboxylate complexes, *Polyhedron* **2005**, *24*, 1185–1195.

- [34] Wojtczak, W. A.; Hampden-Smith, M. J.; Duesler, E. N. Synthesis, characterization, and thermal behavior of polydentate ligand adducts of barium trifluoroacetate, *Inorg. Chem.* **1998**, *37*, 1781-1790.
- [35] Wojtczak, W. A.; Atanassova, P.; Hampden-Smith, M. J.; Duesler, E. Synthesis and characterization of polyether adducts of barium and strontium carboxylates and their use in the formation of MTiO<sub>3</sub> films, *Inorg. Chem.* **1996**, *35*, 6995.
- [36] Mishra, S.; Hubert-Pfalzgraf, L. G.; Daniele, S.; Rolland, M.; Jeanneau, E.; Jouguet, B. Thermal dehydration of [Y(TFA)<sub>3</sub>(H<sub>2</sub>O)<sub>3</sub>]: Synthesis and molecular structures of [Y(μ,η<sup>1</sup>:η<sup>1</sup>-TFA)<sub>3</sub>(THF)(H<sub>2</sub>O)]<sub>1∞</sub>·THF and [Y<sub>4</sub>(μ<sub>3</sub>-OH)<sub>4</sub>(μ,η<sup>1</sup>:η<sup>1</sup>-TFA)<sub>6</sub>(η<sup>1</sup>-TFA)(η<sup>2</sup>-TFA)(THF)<sub>3</sub>(DMSO)(H<sub>2</sub>O)]·6THF, *Inorg. Chem. Commun.* **2009**, *12*, 97-100.
- [37] Mishra, S.; Jeanneau, E.; Ledoux, G.; Daniele, S. Novel barium-organic incorporated iodometallates: Do they have template properties for constructing rare heterotrimetallic hybrids? *Inorg. Chem.* **2014**, *53*, 11721-11731.
- [38] Zhang, J.; Morlens, S.; Hubert-Pfalzgraf, L. G.; Luneau, D. Synthesis, characterization and molecular structures of yttrium trifluoroacetate complexes with O- and N-donors: Complexation vs. hydrolysis, *Eur. J. Inorg. Chem.* **2005**, 3928–3935.
- [39] Mishra, S.; Jeanneau, E.; Bulin, A.-L.; Ledoux, G.; Jouguet, B.; Amans, D.; Belsky, A.; Daniele, S.; Dujardin, C. A molecular precursor approach to monodisperse scintillating CeF<sub>3</sub> nanocrystals, *Dalton Trans.* **2013**, *42*, 12633–12643.
- [40] a) Mosiadz, M.; Judaa, K. L.; Hopkins, S. C.; Soloduch, J.; Glowacki, B. A. An in-depth in situ IR study of the thermal decomposition of barium trifluoroacetate hydrate, *Thermochim. Acta* **2011**, *513*, 33–37; b) Mosiadz, M.; Judaa, K. L.; Hopkins, S. C.; Soloduch, J.; Glowacki, B. A. An in-depth in situ IR study of the thermal decomposition of yttrium trifluoroacetate hydrate, *J. Therm. Anal. Calorim.* **2012**, *107*, 681–691.

- [41] Ledoux, G.; Joubert, M. F.; Mishra, S. Upconversion phenomena in nanofluorides. In *Photonic and electronic properties of fluoride materials*; Tressaud, A., Poepelmeier, K., Eds.; Elsevier: Boston, 2016; pp 35–63.
- [42] a) Johnson, L. F.; Guggenheim, H. J.; Rich, T. C.; Ostermayer, F. W. Infrared-to-visible conversion by rare-earth ions in crystals, *J. Appl. Phys.* **1972**, *43*, 1125 ; b) Guggenheim, H. J.; Johnson, L. F. New Fluoride compounds for efficient infrared-to-visible conversion, *Appl. Phys. Lett.* **1969**, *15*, 51.
- [43] Rabouw, F. T.; Prins, P. T.; Villanueva-Delgado, P.; Castelijns, M.; Geitenbeek, R. G.; Meijerink, A. Quenching pathways in NaYF<sub>4</sub>:Er<sup>3+</sup>,Yb<sup>3+</sup> upconversion nanocrystals. *ACS Nano* **2018**, *12*, 4812–4823.
- [44] *CrysAlisPro Software system*; Rigaku Oxford Diffraction, **2019**, version 1.171.40.67a, Rigaku Corporation, Oxford, UK.
- [45] Clark, R. C.; Reid, J. S. The analytical calculation of absorption in multifaceted crystals. *Acta Crystallogr., Sect. A: Found. Crystallogr.* **1995**, *51*, 887-897.
- [46] Sheldrick, G. M. Crystal structure refinement with ShelXL, *Acta Crystallogr., Sect. C: Struct. Chem.* **2015**, *71*, 3-8.
- [47] Dolomanov O. V., Bourhis L. J., Gildea R. J., Howard J. A. K.; Puschmann, H. *J. Appl. Cryst.* **2009**, *42*, 339-341.
- [48] a) Gahlot, S.; Purohit, B.; Jeanneau, E.; Mishra, S. Coinage metal complexes with di-tertiary-butyl sulfide as precursors with ultra-low decomposition temperature, *Chem. Eur. J.* **2021**, *27*, 10826–10832; b) Gahlot, S.; Jeanneau, E.; Singh, D.; Panda, P. K.; Mishra, Y. K.; Ahuja, R.; Ledoux, G.; Mishra, S. Molecules versus nanoparticles: Identifying a reactive molecular intermediate in the synthesis of ternary coinage metal chalcogenides, *Inorg. Chem.* **2020**, *59*, 7727-7738; c) Gahlot, S.; Jeanneau, E.; Dappozze, F.; Guillard, C.; Mishra, S.

Precursor-mediated synthesis of  $\text{Cu}_{2-x}\text{Se}$  nanoparticles and their composites with  $\text{TiO}_2$  for improved photocatalysis, *Dalton Trans.* **2018**, 47, 8897–8905.

## TOC figure

